# Prediction and Verification of the Structural Chemistry of New One-Dimensional Barium/Copper/Iridium Oxides

Graeme R. Blake,[†] Jeremy Sloan,[†,‡] Jaap F. Vente,[†] and Peter D. Battle*,[†]

*Inorganic Chemistry Laboratory, University of Oxford, South Parks Road, Oxford OX1 3QR, U.K., and Department of Materials, University of Oxford, Parks Road, Oxford OX1 3PH, U.K.*

*Received April 30, 1998. Revised Manuscript Received August 4, 1998*

We propose a classification scheme for the commensurate phases in the family of pseudo one-dimensional structures formed from the mixed hcp stacking of $A_3O_9$ and oxygen-deficient $A_3A'O_6$ layers. We envisage these compounds as composites of two substructures having common *a* and *b* unit cell parameters but different parameters $c_1$ and $c_2$. Use of the ratio $c_1/c_2$ facilitates the prediction of new commensurate structures while allowing for the commonly incommensurate nature of materials in this family. The structures of the new commensurate phases $Ba_5CuIr_3O_{12}$, $Ba_{14}Cu_3Ir_8O_{33}$, $Ba_{16}Cu_3Ir_{10}O_{39}$, and $Ba_9Cu_2Ir_5O_{21}$ are predicted and subsequently verified by powder X-ray diffraction and HRTEM. $Ba_5CuIr_3O_{12}$ has a 10 layer structure with space group *P*321, $a = 10.143\,82(8)$ Å, $c = 21.6553(2)$ Å; $Ba_{14}Cu_3Ir_8O_{33}$ has a 14 layer structure with space group *P*321, $a = 10.145\,85(8)$ Å, $c = 29.9574(3)$ Å; $Ba_{16}Cu_3Ir_{10}O_{39}$ has a 16 layer structure with space group *P*321, $a = 10.136\,43(7)$ Å; $c = 35.0616(3)$ Å; $Ba_9Cu_2Ir_5O_{21}$ has an 18 layer structure with space group *R*32, $a = 10.144\,64(11)$ Å, $c = 38.2455(6)$ Å. Sequences of trigonal prismatic sites and octahedral sites run in chains parallel to *z*, with Ba cations located between the chains; the distribution of iridium and copper cations in the octahedral and trigonal prismatic sites is disordered in each case. Electron diffraction patterns and lattice images show evidence for modulation in the structures of $Ba_5CuIr_3O_{12}$, $Ba_{14}Cu_3Ir_8O_{33}$, and $Ba_{16}Cu_3Ir_{10}O_{39}$ but not in that of $Ba_9Cu_2Ir_5O_{21}$. The magnetic susceptibilities of all four phases obey a modified Curie−Weiss law above 150 K, with no long-range magnetic order observed between 5 and 300 K. They are all electrical insulators.

## Introduction

We have recently reported the crystal structures of $Ba_6CuIr_4O_{15}$ [1] and $Sr_4CuIr_2O_9$.[2] It is convenient to think of these structures (Figure 1) as being derived from an hcp stack (*aba*) of pseudo close packed layers of stoichiometry $A_3O_9$, (A = Sr, Ba). If the octahedral interstices between such layers are filled by cations, B, then the 2H perovskite structure of, for example, $BaNiO_3$,[3] results. An ordered removal of groups of three oxide ions from one of these layers modifies the stoichiometry of that layer to $A_3O_6$, while creating potential cation sites within the layer. These new sites are equidistant from three anions in each of the neighboring layers, and they consequently have trigonal prismatic coordination geometry. When the trigonal prismatic sites are occupied by a cation A′, the stoichiometry of the layer is changed to $A_3A'O_6$ (Figure 2). Darriet and Subramanian[4] discussed the stoichiometries that can arise when a mixed stack of $A_3O_9$ layers and $A_3A'O_6$ layers forms the basis of a crystal structure, the octahedral interstices being occupied by B cations. They described these compounds with the general formula $A_{3n+3}A'_nB_{n+3}O_{6n+9}$, where the layer sequence is $(A_3A'O_6)_n(A_3O_9)$; that is, an $A_3O_9$ layer is inserted after every *n* $(A_3A'O_6)$ layers. $Ba_6CuIr_4O_{15}$ then corresponds to an $n = 1$ structure, $Sr_4CuIr_2O_9$ has $n = 3$ and $Sr_4IrO_6$ (A = A′ = Sr)[5] is the $n = \infty$ end-

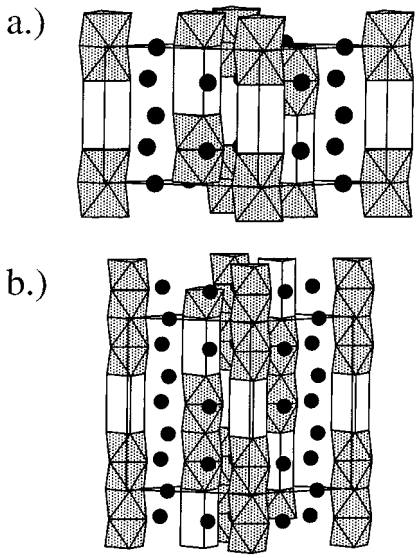


**Figure 1.** Crystal structures of (a) $Sr_4CuIr_2O_9$ and (b) $Ba_6CuIr_4O_{15}$. $IrO_6$ octahedra are shaded; Cu-containing trigonal prismatic sites are unshaded. Black circles represent Sr or Ba.

* To whom correspondence should be addressed.
[†] Inorganic Chemistry Laboratory.
[‡] Department of Materials.

(1) Battle, P. D.; Blake, G. R.; Darriet, J.; Gore, J. G.; Weill, F. *J. Mater. Chem.* **1997**, *7*, 1559.
(2) Battle, P. D.; Blake, G. R.; Sloan, J.; Vente, J. F. *J. Solid State Chem.* **1998**, *136*, 103.
(3) Lander, J. J. *Acta Crystallogr.* **1951**, *4*, 148.
(4) Darriet, J.; Subramanian, M. A. *J. Mater. Chem.* **1995**, *5*, 543.

10.1021/cm980317m CCC: $15.00 © 1998 American Chemical Society
Published on Web 10/15/1998

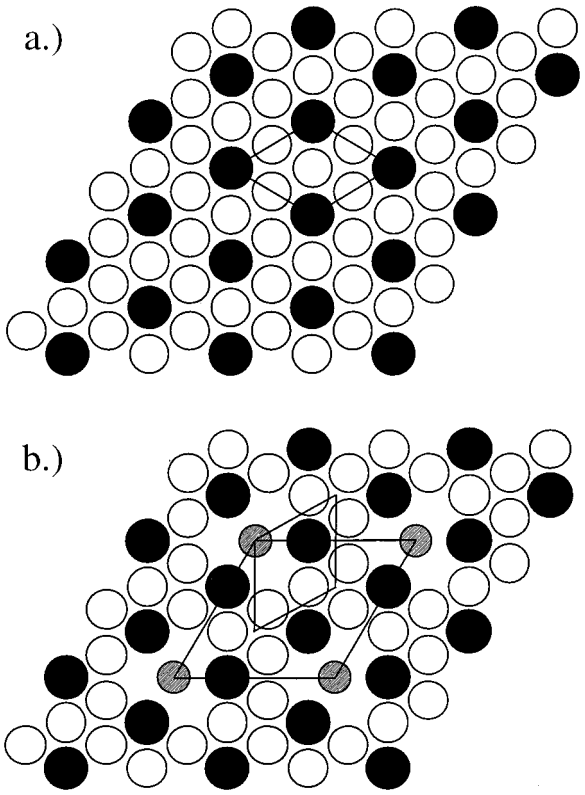


**Figure 2.** Layers of different stoichiometry in $A_{3n+3}A'_nB_{n+3}O_{6n+9}$: (a) an $A_3O_9$ layer, (b) an $A_3O_6$ layer with trigonal prismatic sites (A′) marked by lightly shaded circles. The two-dimensional unit cells of both layer types are shown, with $a' = \sqrt{3}a$.

member of the series; examples involving other transition elements are known and have been listed elsewhere.[6] In an alternative but equivalent view, each of these structures can be described in a trigonal unit cell with three chains of cation-containing polyhedra running parallel to the *z* axis. All of the chains contain the same sequence of $BO_6$ octahedra and $A'O_6$ prisms, but there is an offset between neighboring chains. The atoms A occupy coordination sites between the chains. Both descriptions of the structure type can be recognized in the structure of $Sr_4CuIr_2O_9$, as drawn in Figure 1. In a number of cases, for example $Ba_6ZnIr_4O_{15}$ and $Ba_4CuIr_2O_9$,[1,2] the descriptions of the structures presented above have proved to be inadequate. X-ray and electron diffraction studies have shown these compounds to be incommensurate along [001], with the precise periodicity strongly dependent on synthesis conditions. Their structures can be described as composites containing two substructures, with the same unit cell parameters *a* and *b* but with different parameters $c_1$ and $c_2$; $c_1$ is associated with the columns of A cations and is the mean separation of equivalent, (i.e. alternate) pseudo close packed planes in the *aba* hcp stack, and $c_2$ is the mean spacing of the cations within the polyhedral chains. The unit cell is commensurate when $pc_1 = qc_2$, that is, $c_1/c_2 = q/p$ (*p*, *q* are integers), and incommensurate when $c_1/c_2$ is not a rational fraction. Consistent with these definitions, there are $2p$ layers, either $A_3O_9$ or $A_3A'O_6$, in the unit cell and *q* polyhedra. Each $A_3O_9$ layer generates one octahedral site per chain, but the insertion of an $A_3A'O_6$ layer generates a prismatic site which takes up twice the space (parallel to [001]) of an octahedral site. If we assume that all of the sites in a chain are to be filled, then if $q \leq 2p$, we must utilize $2p - q$ prismatic sites and $2q - 2p$ octahedral sites in order to have a total of *q* sites, all filled. The unit cell of the 2H perovskite ($n = 0$) has two layers and two transition metal cations per chain per unit cell, and therefore $p = 1$, $q = 2$, and $q = 2p$; no prismatic sites are formed, and the structure contains only $A_3O_9$ layers. At the other extreme, $Sr_3A'IrO_6$ ($n = \infty$) has six layers and four cations per chain per unit cell;[5] therefore $p = 3$, $q = 4$, $q = 4p/3$, and equal numbers of octahedral and prismatic sites are utilized. These two limiting cases demonstrate that $(4p/3) \leq q \leq 2p$. For the $A_4A'Ir_2O_9$ ($n = 3$) compounds, $p = 2$, $q = 3$, and we expect $c_1/c_2 = 3/2$ for a commensurate phase; deviations from this value indicate an incommensurate structure. In a similar way, the $n = 1$ structure adopted by $Ba_6CuIr_4O_{15}$ has $c_1/c_2 = 5/3$,[1] whereas the related incommensurate compound $Ba_6ZnIr_4O_{15}$ has $c_1/c_2 = 1.63$.

The use of the parameters *p* and *q* allows us to account for all compounds in the series formulated as $A_{3n+3}A'_nB_{n+3}O_{6n+9}$ by Darriet and Subramanian (DS), and, in addition, it establishes criteria for (in)commensurability among these phases. Furthermore, it enables us to predict new phases which lie outside the original formulation. The description of the stacking sequence as $(A_3A'O_6)_n(A_3O_9)$ limits the model to compositions in which only single $A_3O_9$ layers occur, but it is easy to conceive of stuctures where multiple $(A_3O_9)$ layers separate sequences of $(A_3A'O_6)$ layers. This paper describes our attempts to predict and subsequently prepare and characterize new phases within this general structural framework. Understanding the crystal chemistry of these complex oxides was a major part of the motivation of this work, but we were also aware that the polyhedral chains might have interesting 1D electronic properties if they could be made with the optimum cation distribution. The principal aim of our experimental program was to prepare new phases which cannot be described by the DS formula and to characterize their electronic properties. To do this, we attempted to occupy the B sites with a transition metal which readily takes oxidation states up to IV and the prismatic sites with a relatively small, divalent transition metal cation. Iridium was selected for the former role, and preliminary experiments led us to conclude that Cu is best suited to occupy the trigonal sites.

**Table 1. Preparation of Ba/Cu/Ir/O Phases**

| compd | temps/°C (firing times/days) |
|---|---|
| $Ba_5CuIr_3O_{12}$ | 1200 °C (3 days) + 1250 °C (1 day) |
| $Ba_{14}Cu_3Ir_8O_{33}$ | 1200 °C (2 days) + 1250 °C (8 days) |
| $Ba_{16}Cu_3Ir_{10}O_{39}$ | 1200 °C (4.5 days) |
| $Ba_9Cu_2Ir_5O_{21}$ | 1200 °C (3 days) + 1250 °C (11 days) + 1300 °C (19 days) + 1310 °C (5 days) + 1320 °C (2 days) |

## Experimental Section

Our attempts to synthesize polycrystalline samples (~1 g) of selected compositions employed the standard methods of solid-state chemistry, with $BaCO_3$, CuO, and Ir metal as starting materials. All syntheses were carried out by heating

(5) Powell, A. V.; Battle, P. D.; Gore, J. G. *Acta Crystallogr.* **1993**, *C49*, 189.
(6) Darriet, J.; Grasset, F.; Battle, P. D. *Mater. Res. Bull.* **1997**, *32*, 139.

**Table 2. Possible Stoichiometries of Compounds Based on the Mixed Stacking of $A_3A'O_6$ and $A_3O_9$ Layers[a]**

| layers per unit cell | $p$ | $q$ | octahedra per chain | prisms per chain | comments | $c_1/c_2$ | sequence of polyhedra: translation of ($^1/_3$, $^2/_3$, $z$) chain[b] |
|---|---|---|---|---|---|---|---|
| 2 | 1 | 2 | 2 | 0 | $ABO_3$ | 2 | $o_2$: **a**, 0 ($n = 0$, *2H structure*) |
| 4 | 2 | 4 | 4 | 0 | *2 × 2H structure* | 2 | |
| | 2 | 3 | 2 | 1 | $A_4A'B_2O_9$ | 3/2 | opo: **a**, $c/4$ ($n = 3$) |
| 6 | 3 | 5 | 4 | 1 | $A_6A'B_4O_{15}$ | 5/3 | $o_2po_2$: **a**, $c/3$ (R, $n = 1$); **b**, $c/6$ |
| | 3 | 4 | 2 | 2 | $A_3A'BO_6$ | 4/3 | popo: **a**, $c/3$ (R, $n = \infty$) |
| 8 | 4 | 7 | 6 | 1 | $A_8A'B_6O_{21}$ | 7/4 | $o_3po_3$: **a**, $3c/8$; **b**, $c/4$; **c**, $c/8$ |
| | 4 | 6 | 4 | 2 | $2 \times A_4A'B_2O_9$ | 3/2 | |
| 10 | 5 | 9 | 8 | 1 | $A_{10}A'B_8O_{27}$ | 9/5 | $o_4po_4$: **a**, $2c/5$; **b**, $3c/10$; **c**, $c/5$; **d**, $c/10$ |
| | 5 | 8 | 6 | 2 | $A_5A'B_3O_{12}$ | 8/5 | $po_3po_3$: **a**, $c/5$; **b**, $c/10$ |
| | 5 | 7 | 4 | 3 | $A_{10}A'_3B_4O_{21}$ | 7/5 | opopopo: **a**, $c/10$ ($n = 9$) |
| 12 | 6 | 11 | 10 | 1 | $A_{12}A'B_{10}O_{33}$ | 11/6 | $o_5po_5$: **a**, $5c/12$; **b**, $c/3$ (R); **c**, $c/4$; **d**, $c/6$; **e**, $c/12$ |
| | 6 | 10 | 8 | 2 | $2 \times A_6A'B_4O_{15}$ | 5/3 | |
| | 6 | 9 | 6 | 3 | $3 \times A_4A'B_2O_9$ | 3/2 | |
| | 6 | 8 | 4 | 4 | $2 \times A_3A'BO_6$ | 4/3 | |
| 14 | 7 | 13 | 12 | 1 | $A_{14}A'B_{12}O_{39}$ | 13/7 | $o_6po_6$: **a**, $3c/7$; **b**, $5c/14$; **c**, $2c/7$; **d**, $3c/14$; **e**, $c/7$; **f**, $c/14$ |
| | 7 | 12 | 10 | 2 | $A_7A'B_5O_{18}$ | 12/7 | $po_5po_5$: **a**, $3c/14$; **b**, $c/7$; **c**, $c/14$ |
| | 7 | 11 | 8 | 3 | $A_{14}A'_3B_8O_{33}$ | 11/7 | $opo_3po_3po$: **a**, $3c/7$; **b**, $3c/14$; **c**, $c/14$ |
| | 7 | 10 | 6 | 4 | $A_7A'_2B_3O_{15}$ | 10/7 | $opopo_2popo$: **a**, $c/14$ ($n = 6$) |
| | | | | | | | $popo_2po_2po$: **b**, $c/14$ |
| 16 | 8 | 15 | 14 | 1 | $A_{16}A'B_{14}O_{45}$ | 15/8 | $o_7po_7$: **a**, $7c/16$; **b**, $3c/8$; **c**, $5c/16$; **d**, $c/4$; **e**, $3c/16$; **f**, $c/8$; **g**, $c/16$ |
| | 8 | 14 | 12 | 2 | $2 \times A_8A'B_6O_{21}$ | 7/4 | |
| | 8 | 13 | 10 | 3 | $A_{16}A'_3B_{10}O_{39}$ | 13/8 | $o_2po_3po_3po_2$: **a**, $7c/16$; **b**, $c/4$; **c**, $c/8$; **d**, $c/16$ |
| | 8 | 12 | 8 | 4 | $4 \times A_4A'B_2O_9$ | 3/2 | |
| | 8 | 11 | 6 | 5 | $A_{16}A'_5B_6O_{33}$ | 11/8 | opopopopopo: **a**, $c/16$ ($n = 15$) |
| 18 | 9 | 17 | 16 | 1 | $A_{18}A'B_{16}O_{51}$ | 17/9 | $o_8po_8$: **a**, $4c/9$; **b**, $7c/18$; **c**, $c/3$ (R); **d**, $5c/18$; **e**, $2c/9$; **f**, $c/6$; **g**, $c/9$; **h**, $c/18$ |
| | 9 | 16 | 14 | 2 | $A_9A'B_7O_{24}$ | 16/9 | $po_7po_7$: **a**, $c/3$ (R); **b**, $c/9$; **c**, $c/18$ |
| | 9 | 15 | 12 | 3 | $3 \times A_6A'B_4O_{15}$ | 5/3 | |
| | 9 | 14 | 10 | 4 | $A_9A'_2B_5O_{21}$ | 14/9 | $opo_3po_2po_3po$: **a**, $c/3$ (R, $n = 2$); **b**, $c/18$ |
| | | | | | | | $po_3po_2po_2po_3$: **c**, $c/3$ (R); **d**, $c/6$; **e**, $c/18$ |
| | 9 | 13 | 8 | 5 | $A_{18}A'_5B_8O_{39}$ | 13/9 | $po_2popo_2popo_2$: **a**, $c/3$ (R, $n = 5$); **b**, $c/18$ |
| | | | | | | | $popo_2po_2po_2po$: **c**, $c/18$ |
| | 9 | 12 | 6 | 6 | $3 \times A_3A'BO_6$ | 4/3 | |

[a] Compositions which can be described as DS phases $(A_3A'O_6)_n(A_3O_9)$ are shown in italics. $c_1/c_2$ is given for a commensurate structure. [b] Sequence of polyhedra ($o_n = n$ adjacent face-sharing octahedra) for the chain along (0,0,$z$) is given, followed by relative translations of the ($^1/_3$, $^2/_3$, $z$) chain to give structures **a**−**c**, etc. (R) denotes rhombohedral structures; all others are trigonal except for 2H.

alumina crucibles containing pelletized, stoichiometric mixtures of the appropriate reactants in air, initially at 800 °C and subsequently as described in Table 1. The progress of the reactions was followed by X-ray powder diffraction (XRD), and they were deemed to be complete when the measured diffraction pattern could be accounted for by the presence of one commensurate phase having trigonal or rhombohedral symmetry. The XRD data were collected at room temperature over the angular range $5 \leq 2\theta/\text{deg} \leq 120$, with a step size of $\Delta 2\theta = 0.02°$, on a Siemens D5000 diffractometer operating with Cu $K\alpha_1$ radiation in Bragg−Brentano geometry. The data were analyzed by the Rietveld method,[7] as implemented in the GSAS program suite.[8] Further structural characterization of the products was carried out using a JEOL-4000EX HRTEM operated at 400 kV. This microscope has a point resolution of 1.7 Å and a spherical aberration coefficient of 9 Å. Finely ground specimens were dispersed in chloroform in an ultrasonic bath and then placed, dropwise, onto lacey carbon-coated copper grids (Agar 200 mesh). Lattice images were recorded under optimum Scherzer defocus conditions from crystal fragments with their [010] or [1$\bar{1}$0] zone axes aligned parallel to the electron beam. Image simulations were calculated using the multislice program in the EMS program package.[9] The metal content of the products was analyzed using an Atomscan 25 ICP emission spectrometer. Magnetic measurements were made on a sample contained in a gelatin capsule using a Quantum Design MPMS-5 SQUID magnetometer. Data were recorded while warming the sample through the temperature range $5 \leq T/\text{K} \leq 300$ after cooling in zero field (ZFC) and after cooling in the measuring fields (100 and 1000 G, FC). Electrical conductivity measurements were attempted using the standard four-probe technique, copper wires being attached to a sintered bar of the sample with conducting silver paint.

**Table 3. Observed (Calculated) Metal Content of Ba/Cu/Ir/O Phases**

| compd | % Ba | % Cu | % Ir |
|---|---|---|---|
| $Ba_5CuIr_3O_{12}$ | 45.02 (45.21) | 4.00 (4.18) | 38.13 (37.97) |
| $Ba_{14}Cu_3Ir_8O_{33}$ | 46.77 (46.01) | 4.41 (4.56) | 37.46 (36.80) |
| $Ba_{16}Cu_3Ir_{10}O_{39}$ | 45.56 (44.53) | 3.66 (3.86) | 39.73 (38.96) |
| $Ba_9Cu_2Ir_5O_{21}$ | 49.31 (46.46) | 4.87 (4.78) | 35.54 (36.13) |

## Results

Two assumptions were made in predicting possible target structures; first, in any one chain, trigonal prismatic sites are always separated by at least one octahedral site and, second, no layer has more than one-third of the oxide ions absent, thus eliminating the possibility that, for a given layer, trigonal prismatic sites can occur in more than one chain. Use of the relationship $(4p/3) \leq q \leq 2p$ for $p \leq 9$ generates the possible stoichiometries listed in Table 2. The choice $p_{max} = 9$ is arbitrary; there is no limit to the number of structures that can be envisaged with a greater number of layers in the unit cell. By way of example, some of the possible 10 layer ($p = 5$) structures are drawn in Figure 3; $A_{10}A'_3B_4O_{21}$ (Figure 3a) can be recognized as a DS $n = 9$ structure with $c_1/c_2 = 7/5$, whereas $A_5A'B_3O_{12}$ (Figure 3b) has $c_1/c_2 = 8/5$ and cannot be described in the DS

(7) Rietveld, H. M. *J. Appl. Crystallogr.* **1969**, *2*, 65.
(8) Larson, A. C. and von Dreele, R. B. *General Structure Analysis System (GSAS)*; Report LAUR 86-748, Los Alamos National Laboratories: Los Alamos, NM, 1990.
(9) Stadelman, P. A. *Ultramicroscopy* **1987**, *21*, 131.

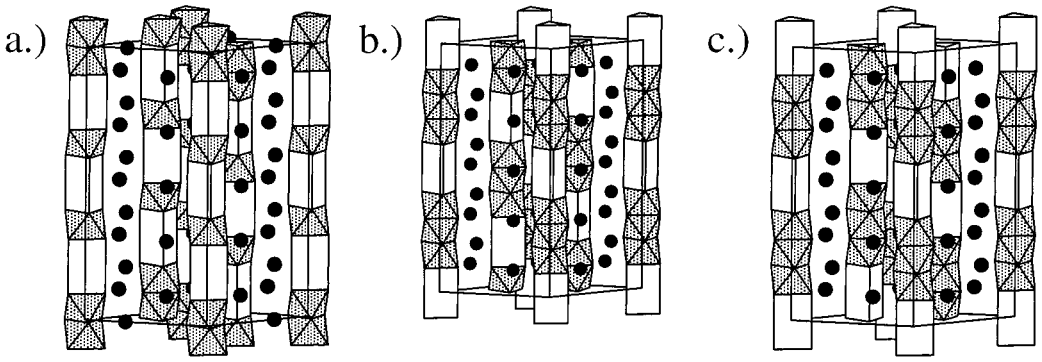


**Figure 3.** Idealized crystal structures of the 10 layer compounds: (a) $A_{10}A'_3B_4O_{21}$; (b) $A_5A'B_3O_{12}$ (model **a**); (c) $A_5A'B_3O_{12}$ (model **b**).

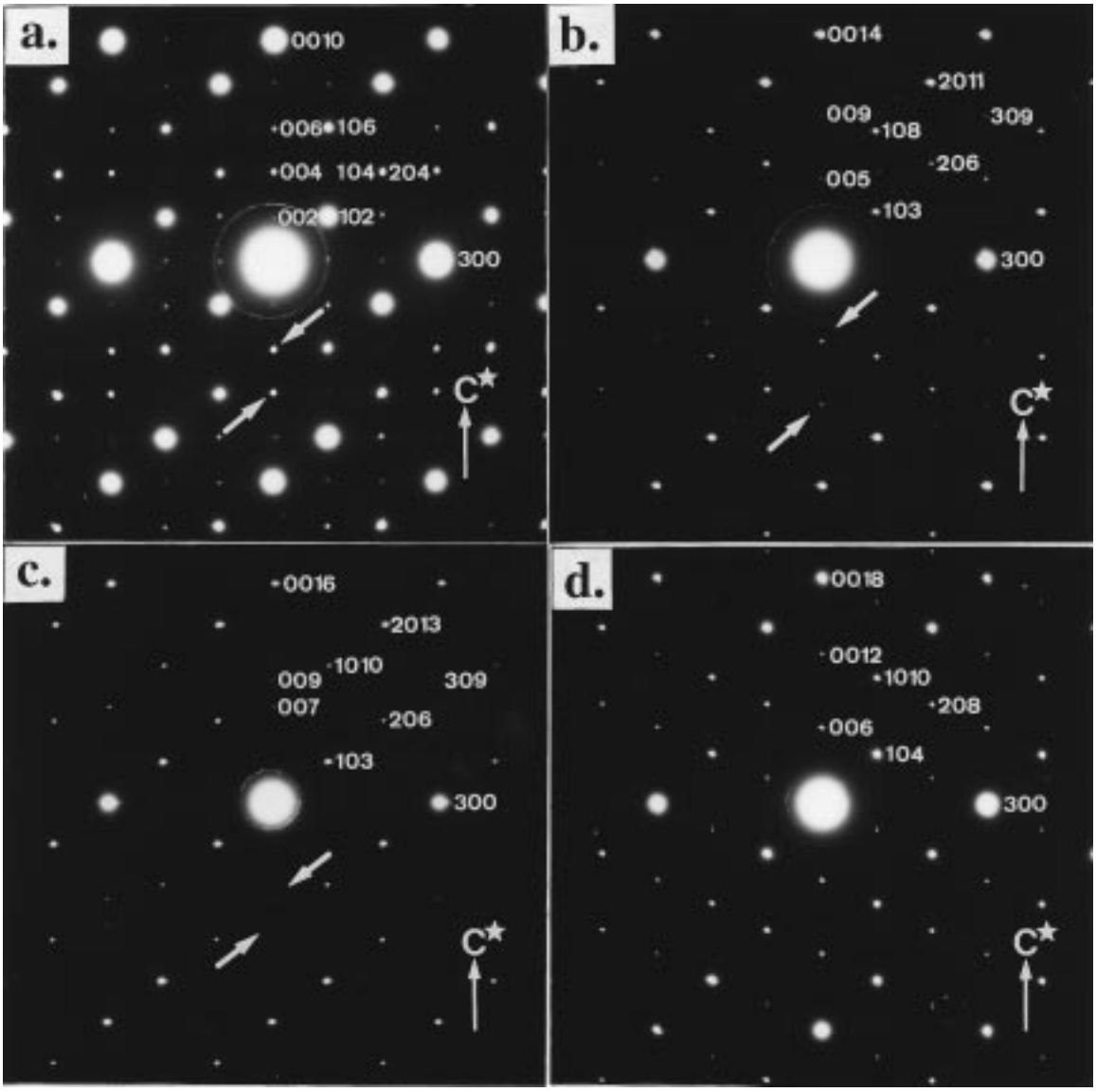


**Figure 4.** [010] zone electron diffraction patterns of (a) $Ba_5CuIr_3O_{12}$, (b) $Ba_{14}Cu_3Ir_8O_{33}$, (c) $Ba_{16}Cu_3Ir_{10}O_{39}$, and (d) $Ba_9Cu_2Ir_5O_{21}$.

**Table 4. Unit Cell Parameters of Ba/Cu/Ir/O Phases from X-ray Diffraction**

| compd | *a*/Å | *c*/Å | $c_1$/Å | $c_2$/Å | $c_1/c_2$ |
|---|---|---|---|---|---|
| $Ba_5CuIr_3O_{12}$ | 10.143 82(8) | 21.6553(2) | 4.3292(7) | 2.7063(3) | 1.5997(5) |
| $Ba_{14}Cu_3Ir_8O_{33}$ | 10.145 85(8) | 29.9574(3) | 4.2800(3) | 2.7225(3) | 1.5721(3) |
| $Ba_{16}Cu_3Ir_{10}O_{39}$ | 10.136 43(7) | 35.0616(3) | 4.3826(8) | 2.6963(4) | 1.6254(5) |
| $Ba_9Cu_2Ir_5O_{21}$ | 10.144 64(11) | 38.2455(6) | 4.2454(6) | 2.7284(3) | 1.5560(4) |

scheme. However, further consideration shows that a second 10 layer structure (Figure 3c) with trigonal symmetry is also consistent with the unit cell dimensions and the composition of the latter phase. In fact,

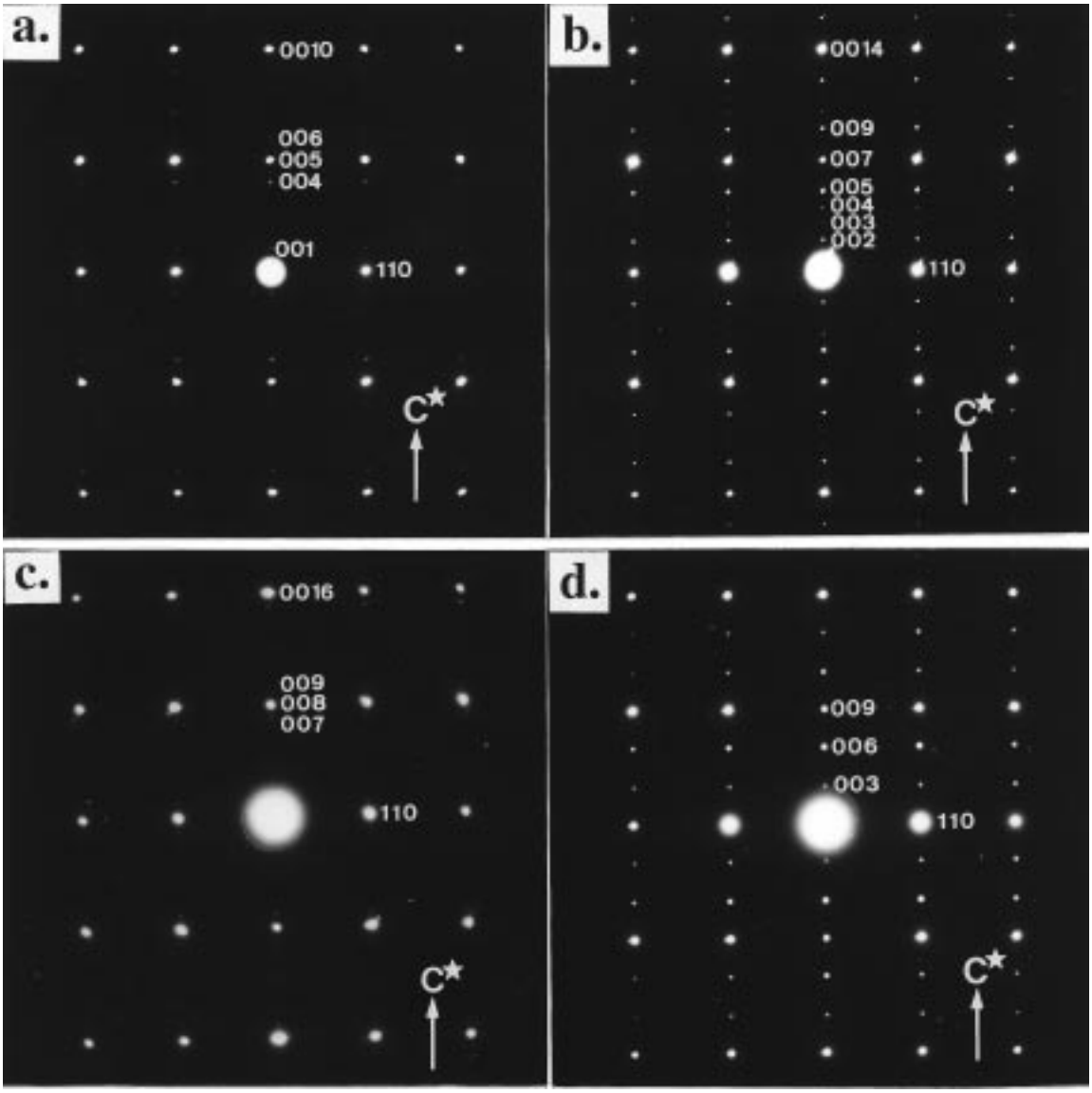


**Figure 5.** [1$\bar{1}$0] zone electron diffraction patterns of (a) $Ba_5CuIr_3O_{12}$, (b) $Ba_{14}Cu_3Ir_8O_{33}$, (c) $Ba_{16}Cu_3Ir_{10}O_{39}$, and (d) $Ba_9Cu_2Ir_5O_{21}$.

not only are there three possible stoichiometries for a 10 layer structure (Table 2, column 6), but in two of the three cases these stoichiometries can be accommodated in a number of subtly different structures (Table 2, column 8). For a particular stoichiometry, the sequence of octahedra and prisms in the individual polyhedral chains is usually the same (there are exceptions for one of the 14 layer phases and two of the 18 layer phases which have more than one possible sequence), but in the different models (**a**, **b**, etc.), the transition metal chains at ($^1/_3$, $^2/_3$, $z$) and ($^2/_3$, $^1/_3$, $z$) are translated by different amounts with respect to the chain at (0, 0, $z$); in a particular model the translations of the former two chains are equal and opposite. Figure 3b is drawn with a translation of $c/5$; the alternative, idealized structure of $A_5A'B_3O_{12}$, with a translation of $c/10$, is shown in Figure 3c. A full breakdown of possible structures for all values of $p$ and $q$ is included in Table 2 (column 8).

We attempted to prepare a number of these predicted structures, and, as implied above in Table 1, we were successful in the cases of 10 layer $Ba_5CuIr_3O_{12}$, 14 layer $Ba_{14}Cu_3Ir_8O_{33}$, 16 layer $Ba_{16}Cu_3Ir_{10}O_{39}$, and 18 layer $Ba_9Cu_2Ir_5O_{21}$. Table 3 lists the metal contents of the reaction products as determined from ICP analysis. The experimental values lead to stoichiometries close to those expected, although the Ba content of $Ba_9Cu_2Ir_5O_{21}$ is rather high. Unfortunately, oxygen contents could not be determined accurately. Thermogravimetric analysis (TGA) using 10% $H_2/N_2$ as the reducing agent was attempted, but the weight losses in the TGA data had poorly defined endpoints for all of the compounds studied. The final X-ray powder diffraction patterns of the compositions listed in Table 1 could all be indexed in commensurate, trigonal, or rhombohedral unit cells. Alternatively, the patterns could be indexed using the composite crystal model described above, in which the two subcells have common $a$, $b$ parameters but distinct $c$ parameters, $c_1$ and $c_2$. The values of the ratio $c_1/c_2$ obtained from the powder XRD data using this approach agree with those expected for each composition (cf. Tables 2 and 4), thus confirming the nature of the reaction product. In all cases a single-phase incommensurate product with $c_1/c_2$ greater than the ideal value formed initially, and the final stages of firing were used to decrease $c_1/c_2$ to the commensurate value. Unsuccessful attempts were also made to prepare the predicted phases $Ba_7CuIr_5O_{18}$ ($c_1/c_2 = 12/7$) and $Ba_8CuIr_6O_{21}$ ($c_1/c_2 = 7/4$); incommensurate products with

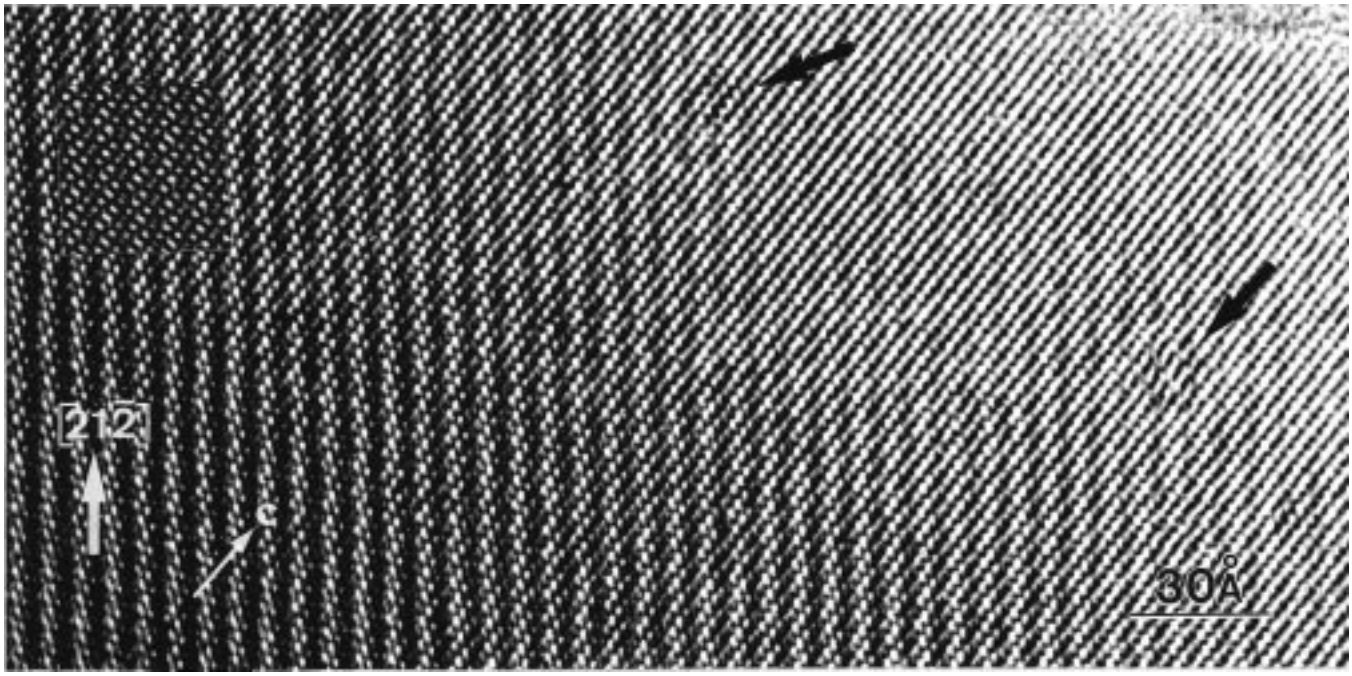


**Figure 6.** [010] zone lattice image of $Ba_5CuIr_3O_{12}$. Black arrows indicate defects caused by beam damage. A simulated image is included (inset).

$c_1/c_2$ lower than the ideal values were obtained, the ratio decreasing further with continued heating.

The results of our electron microscopy give further insight into the structures of these materials. All electron diffraction patterns were consistent with the indexing of the X-ray diffraction data; the [010] zones for $Ba_5CuIr_3O_{12}$, $Ba_{14}Cu_3Ir_8O_{33}$, and $Ba_{16}Cu_3Ir_{10}O_{39}$, shown in Figure 4a−c respectively, and the [1$\bar{1}$0] zones, shown in Figure 5a−c, show trigonal symmetry, but they do not obey the reflection condition (00$l$), $l = 2n$, thus indicating the absence of glide planes. Figures 4d and 5d show the [010] and [1$\bar{1}$0] zones of $Ba_9Cu_2Ir_5O_{21}$. For this compound the centring condition $-h + k + l = 3n$ is obeyed, indicating rhombohedral symmetry, although the reflection condition (00$l$), $l = 6n$, is not obeyed, indicating the absence of glide planes. In all diffraction patterns except those of $Ba_9Cu_2Ir_5O_{21}$ the intensity distribution of the reflections resembled that observed previously from related incommensurate phases, for example, $Ba_6ZnIr_4O_{15}$,[1] which generate both a set of principal reflections and a second set of generally less intense satellites. However, all of the reflections in our electron diffraction patterns, even those which are apparently satellites, could be indexed in conventional three-dimensional unit cells, confirming that the new phases are commensurate. In Figure 4a−c rows of reflections (arrowed) may be seen to reach a maximum in intensity and then to diminish to zero—a characteristic feature of modulated structures, which is absent from Figure 4d. The intense reflections (00(2$p$)), where 2$p$ is the number of layers in the unit cell, are a distinctive feature of all four of the [010] and [1$\bar{1}$0] zones observed, and they correspond to the (0020) reflection in the composite crystal model; that is, they lie a distance of $2c_1^*$ from the origin of reciprocal space. The apparent modulation vector $\mathbf{q} = \mathbf{a}^* + n\mathbf{c}_1^*$ may then be determined from the [010] zones, and in all cases $n$ is found to be a rational fraction, indicating a commensurate structure.

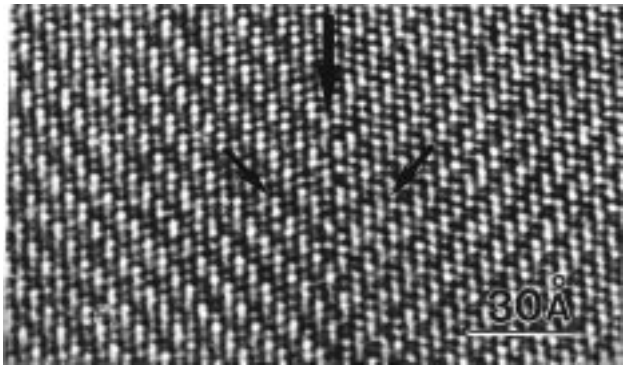


**Figure 7.** [010] zone lattice image of $Ba_{16}Cu_3Ir_{10}O_{39}$. The vertical arrow parallel to $c$ indicates a twin boundary, and the diagonal arrows indicate bands of light and dark contrast on either side of the twin boundary.

The [010] lattice images of $Ba_5CuIr_3O_{12}$ and $Ba_{16}Cu_3Ir_{10}O_{39}$ are shown in Figures 6 and 7, respectively. Figure 6 is typical of a [010] zone lattice image for phases in this family. On the right-hand side of the image regularly spaced lattice fringes, parallel to [001], can be seen. On the left-hand side, light and dark bands parallel to [21$\bar{2}$] are superimposed on the underlying pattern. A notable feature is the formation of small defects, the positions of which are indicated by black arrows. These defects are probably a result of beam damage; all of our phases were beam sensitive and began to deteriorate within minutes when irradiated by high-energy electrons. The [010] zone lattice image of $Ba_{16}Cu_3Ir_{10}O_{39}$ in Figure 7 shows a twin boundary running parallel to $c$ (vertical arrow). The diagonal arrows indicate parallel fringes of dark and light contrast, running parallel to [213] and [21$\bar{3}$].

The [1$\bar{1}$0] zone lattice images of $Ba_5CuIr_3O_{12}$, $Ba_{14}Cu_3Ir_8O_{33}$, $Ba_{16}Cu_3Ir_{10}O_{39}$, and $Ba_9Cu_2Ir_5O_{21}$ are shown in Figure 8a−d, respectively. The first three phases display modulation of image contrast with dark bands superimposed on the lattice images in a direction

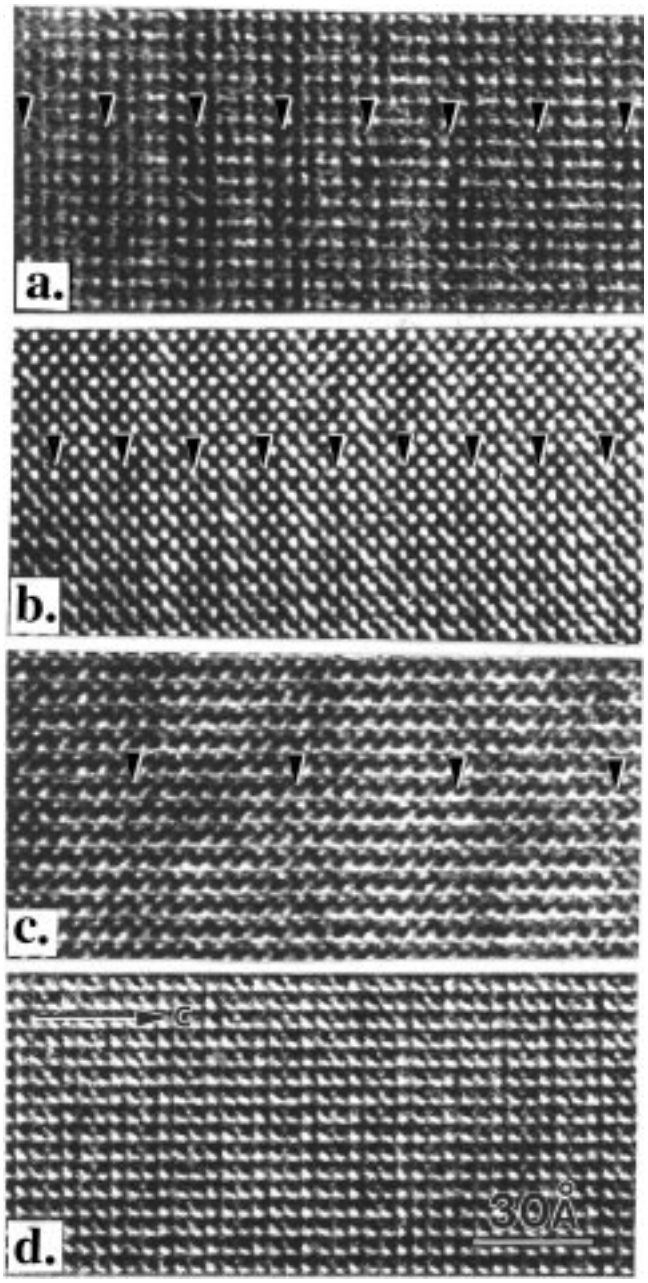


**Figure 8.** [1$\bar{1}$0] zone lattice images of (a) $Ba_5CuIr_3O_{12}$, (b) $Ba_{14}Cu_3Ir_8O_{33}$, (c) $Ba_{16}Cu_3Ir_{10}O_{39}$, and (d) $Ba_9Cu_2Ir_5O_{21}$. Contrast modulation is apparent in (a−c); bands of darker contrast are indicated by arrows.

perpendicular to *c*. This is best observed at a glancing angle at 90° to the *c* direction, and arrows have been placed to show the areas of darker contrast. The images were recorded for crystals of varying thickness, and, as a result, the substructure appears differently in each case. The positions of the contrast modulations were, however, found to be independent of crystal thickness or defocus. In Figure 8d ($Ba_9Cu_2Ir_5O_{21}$) there are sharper dark lines which appear at intervals of *c*/3 and result simply from the basic crystal structure. As in the electron diffraction data, the lattice image of this phase does not show modulation in the same manner as the other three. For $Ba_5CuIr_3O_{12}$, $Ba_{14}Cu_3Ir_8O_{33}$, and $Ba_{16}Cu_3Ir_{10}O_{39}$ the periods of contrast modulation correspond approximately to *c*, *c*/2, and *c*, respectively. These observations indicate that, for these three phases, there is a periodic fluctuation of electron density which is commensurate with *c*.

Having established that the diffraction patterns of our reaction products were consistent with the basic structural principles outlined above, we began to analyze their crystal chemistry in more detail. The two candidate structures, **a** and **b**, for 10 layer $Ba_5CuIr_3O_{12}$ are shown in Figure 3b,c. It should be noted that a similar 10 layer phase has recently been observed by TEM for the compound $Sr_5Co_4O_{12}$,[10] and the structure proposed was that of Figure 3b. Rietveld refinements were carried out in the space group *P*321 using both possible structures of $Ba_5CuIr_3O_{12}$ as starting models. The refinement of model **a** gave slightly better results and will be described below. Initially the $Ir^{4+}$ cations were assigned to the octahedral sites and the $Cu^{2+}$ cations to the trigonal prismatic sites. However, a difference Fourier map suggested that the latter were displaced off the 3-fold axis running along the center of the polyhedral chains and toward the rectangular faces of the trigonal prisms. Least squares refinement showed that only two of the four $Cu^{2+}$ cations were disordered in this way, from the 1b and 2d to 3f and 6g positions, respectively, with occupancies of 1/3. The distribution of $Cu^{2+}$ and $Ir^{4+}$ cations over the octahedral and prismatic sites was also refined, and the introduction of these two forms of disorder led to a significant improvement in the agreement between the observed and calculated diffraction profiles. The best fit was obtained by fixing the Ir occupancy in the central octahedra of the trimers to 100%. The oxygen atomic coordinates were refined, initially by use of soft constraints to give chemically reasonable cation−oxygen bond distances, and finally by the unconstrained refinement of each oxide ion in turn. Attempts at simultaneous unconstrained refinement of all oxygen atomic coordinates led to divergence with some cation−oxygen bond distances within the polyhedra becoming unrealistically short. The atomic coordinates for oxygen tabulated below were thus not obtained from a full-matrix least squares refinement, and we omit bond distances and standard deviations for oxygen coordinates to emphasize the limitations of our structure determination. The best refinements were obtained when preferred orientation effects were allowed for. The refinement of model **b** proceeded in very similar fashion, but the agreement between observed and calculated diffraction profiles was slightly worse (Rwpr = 14.86%, $\chi^2$ = 2.58 as opposed to Rwpr = 14.37%, $\chi^2$ = 2.41 for model **a**), and the Ir/Cu distribution was slightly more disordered. Bond distances were similar in each case. The refined structural parameters for model **a** are listed in Table 5, with the diffraction profiles plotted in Figure 9. The approximate coordinates of model **b** can be generated from those of model **a** by the application of the appropriate translations. The [010] zone lattice image offers further support for this structural model. The view of the structure in Figure 10 shows that the high electron density $Ir_3O_{12}$ trimers and the relatively low-density $CuO_6$ trigonal prisms align parallel to [21$\bar{2}$] (arrowed), the direction in which light and dark bands are obvious in the lattice image of Figure 6. Furthermore, the lattice image simulated

(10) Christoffersen, R.; Jacobson, A. J.; Hegwood, S. L.; Liu, L. *Mater. Res. Soc. Symp. Proc.* **1997**, *453*, 153.

**Table 5. Atomic Parameters for $Ba_5CuIr_3O_{12}$ (Model a)[a]**

| atom | site | Ir fraction[b] | *x* | *y* | *z* | $U_{iso}$/Å$^2$ |
|---|---|---|---|---|---|---|
| Ba1 | 3e | | 0 | 0.350(3) | 0 | 0.0045(6) |
| Ba2 | 6g | | 0.326(3) | 0.339(3) | 0.0967(8) | 0.0045(6) |
| Ba3 | 6g | | 0.007(2) | 0.328(3) | 0.1968(6) | 0.0045(6) |
| Ba4 | 6g | | 0.334(3) | 0.318(2) | 0.2987(7) | 0.0045(6) |
| Ba5 | 6g | | 0.001(3) | 0.342(3) | 0.3943(7) | 0.0045(6) |
| Ba6 | 3f | | 0.347(4) | 0.347(4) | 1/2 | 0.0045(6) |
| Ir1/Cu1 | 2c | 0.788(7) | 0 | 0 | 0.1306(12) | 0 |
| Ir2/Cu2 | 2c | 1.0 | 0 | 0 | 0.2508(10) | 0 |
| Ir3/Cu3 | 2c | 0.788(7) | 0 | 0 | 0.3723(11) | 0 |
| Ir4/Cu4 | 2d | 1.0 | 1/3 | 2/3 | 0.0433(10) | 0 |
| Ir5/Cu5 | 2d | 0.788(7) | 1/3 | 2/3 | 0.1662(10) | 0 |
| Ir6/Cu6 | 2d | 0.788(7) | 1/3 | 2/3 | 0.4244(10) | 0 |
| Ir7/Cu7 | 2d | 1.0 | 1/3 | 2/3 | 0.5446(11) | 0 |
| Ir8/Cu8 | 2d | 0.788(7) | 1/3 | 2/3 | 0.6637(11) | 0 |
| Ir9/Cu9 | 2d | 0.788(7) | 1/3 | 2/3 | 0.9266(11) | 0 |
| Ir10/Cu10 | 1a | 0.425(13) | 0 | 0 | 0 | 0.009(4) |
| Ir11/Cu11 | 3f | 0.141(4) | 0.075(7) | 0 | 1/2 | 0.009(4) |
| Ir12/Cu12 | 6g | 0.141(4) | 0.420(4) | 2/3 | 0.295(2) | 0.009(4) |
| Ir13/Cu13 | 2d | 0.425(13) | 1/3 | 2/3 | 0.7828(14) | 0.009(4) |
| O1 | 6g | | 0.306 | 0.498 | 0.988 | 0 |
| O2 | 6g | | 0.005 | 0.150 | 0.074 | 0 |
| O3 | 6g | | 0.356 | 0.848 | 0.112 | 0 |
| O4 | 6g | | 0.854 | 0.406 | 0.154 | 0 |
| O5 | 6g | | 0.837 | 0.000 | 0.193 | 0 |
| O6 | 6g | | 0.349 | 0.515 | 0.220 | 0 |
| O7 | 6g | | 0.009 | 0.172 | 0.309 | 0 |
| O8 | 6g | | 0.849 | 0.380 | 0.276 | 0 |
| O9 | 6g | | 0.866 | 0.034 | 0.427 | 0 |
| O10 | 6g | | 0.320 | 0.503 | 0.374 | 0 |
| O11 | 6g | | 0.685 | 0.180 | 0.393 | 0 |
| O12 | 6g | | 0.349 | 0.832 | 0.487 | 0 |

[a] Space group *P*321; $a = 10.143\ 82(8)$ Å; $c = 21.6553(2)$ Å; $V = 1929.73(4)$ Å$^3$. [b] Ir fraction + Cu fraction = 1, except Ir/Cu11,12, where $\Sigma = 0.333$; Rwpr = 14.37%, Rp = 11.38%, and $\chi^2 = 2.414$. No standard deviations for oxygen atomic coordinates are shown as they were refined individually and then fixed; $U_{iso}$ for O and Cu/Ir in octahedral sites were fixed at zero.

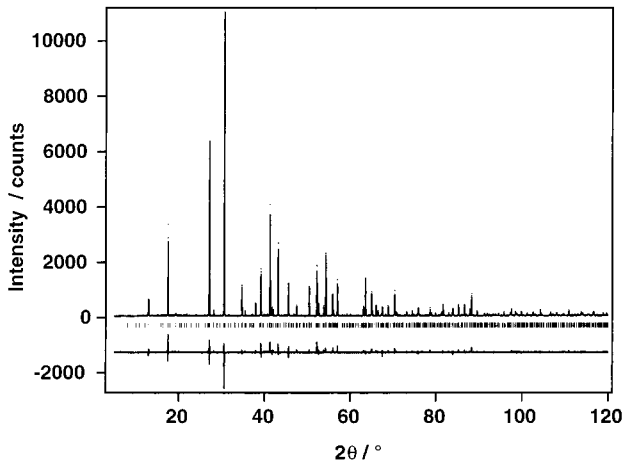


**Figure 9.** Observed, calculated, and difference X-ray diffraction profiles of $Ba_5CuIr_3O_{12}$. Reflection positions are marked.

from our refined atomic coordinates, with a defocus of −680 Å and a foil thickness of 26.3 Å, overlies the observed image very well, thus demonstrating that these bands are a consequence of the basic crystal structure and not a consequence of modulation. The image calculated from model **b** gives slightly inferior agreement.

From Table 2, there are three possible structures for 14 layer $Ba_{14}Cu_3Ir_8O_{33}$, one of which (**b**) is shown in Figure 11. Structural refinements were carried out (space group *P*321) using all three structures as starting models, and they each required the introduction of the same types of disorder as were described above for $Ba_5CuIr_3O_{12}$. In terms of agreement between observed and calculated diffraction profiles, there was little to choose between models **a** and **b**, although model **c** can be rejected. We list the refined coordinates of model **b** ($R_{wpr} = 12.44\%$, $\chi^2 = 1.523$) in Table 6; approximate coordinates of model **a** can be generated by applying the appropriate translations; the Ir/Cu distribution is essentially the same in both models.

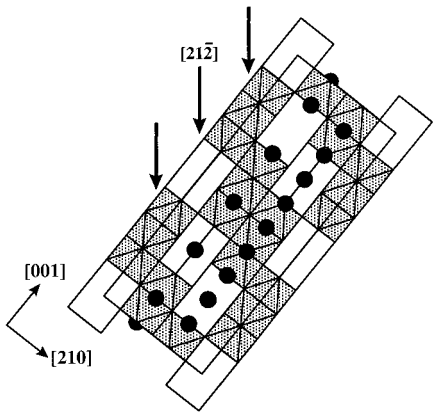


**Figure 10.** View along [010] of the idealized crystal structure of $Ba_5CuIr_3O_{12}$. Arrows indicate parallel bands of high electron density ($Ir_3O_{12}$ trimers) and relatively low density ($CuO_6$ trigonal prisms) along the [21$\bar{2}$] crystal direction, as seen in the [010] zone lattice image of Figure 6.

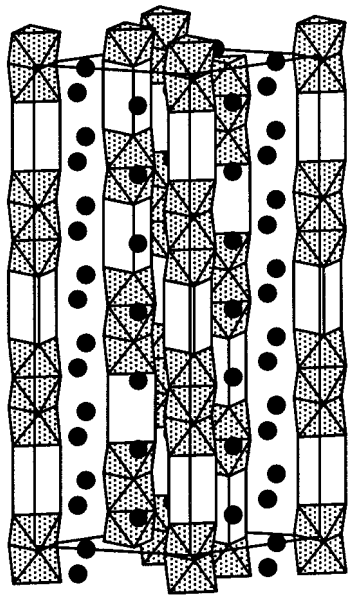

**Figure 11.** Plausible (model **b**) crystal structure of $Ba_{14}Cu_3Ir_8O_{33}$. Octahedra are shaded; trigonal prismatic sites are unshaded. Shaded circles represent Ba.

The four possible structures for 16 layer $Ba_{16}Cu_3Ir_{10}O_{39}$ are described in Table 2, and one of them (model **c**) is drawn in Figure 12. Refinements in space group *P*321 progressed in a fashion similar to those of the phases described above and showed that model **d** may be rejected. However, they were unable to distinguish between models **a**−**c**. The refined structural parameters for model **c** ($R_{wpr} = 10.43\%$, $\chi^2 = 1.041$) are presented in Table 7.

In the case of $Ba_9Cu_2Ir_5O_{21}$, Table 2 shows that there are five possible structures available to an 18 layer compound with this composition; models **a** and **c** have rhombohedral symmetry, whereas models **b**, **d**, and **e**

**Table 6. Atomic Parameters for $Ba_{14}Cu_3Ir_8O_{33}$ (Model b)**

| atom | site | Ir fraction[a] | *x* | *y* | *z* | $U_{iso}$/Å$^2$ |
|---|---|---|---|---|---|---|
| Ba1 | 3e | | 0 | 0.330(5) | 0 | 0.0109(6) |
| Ba2 | 6g | | 0.336(4) | 0.317(4) | 0.0714(8) | 0.0109(6) |
| Ba3 | 6g | | 0.997(4) | 0.343(4) | 0.1439(8) | 0.0109(6) |
| Ba4 | 6g | | 0.331(4) | 0.340(3) | 0.2143(11) | 0.0109(6) |
| Ba5 | 6g | | 0.024(3) | 0.337(3) | 0.2837(9) | 0.0109(6) |
| Ba6 | 6g | | 0.333(4) | 0.322(4) | 0.3563(9) | 0.0109(6) |
| Ba7 | 6g | | 0.984(3) | 0.317(3) | 0.4311(6) | 0.0109(6) |
| Ba8 | 3f | | 0.343(4) | 0.343(4) | $^1/_2$ | 0.0109(6) |
| Ir1/Cu1 | 2c | 0.779(6) | 0 | 0 | 0.0417(9) | 0.0007(6) |
| Ir2/Cu2 | 2c | 0.779(6) | 0 | 0 | 0.2352(9) | 0.0007(6) |
| Ir3/Cu3 | 2c | 1.0 | 0 | 0 | 0.3186(9) | 0.0007(6) |
| Ir4/Cu4 | 2c | 0.779(6) | 0 | 0 | 0.4067(8) | 0.0007(6) |
| Ir5/Cu5 | 2d | 0.779(6) | $^1/_3$ | $^2/_3$ | 0.1652(11) | 0.0007(6) |
| Ir6/Cu6 | 2d | 0.779(6) | $^1/_3$ | $^2/_3$ | 0.2587(10) | 0.0007(6) |
| Ir7/Cu7 | 2d | 0.779(6) | $^1/_3$ | $^2/_3$ | 0.4420(10) | 0.0007(6) |
| Ir8/Cu8 | 2d | 1.0 | $^1/_3$ | $^2/_3$ | 0.5308(8) | 0.0007(6) |
| Ir9/Cu9 | 2d | 0.779(6) | $^1/_3$ | $^2/_3$ | 0.6181(10) | 0.0007(6) |
| Ir10/Cu10 | 2d | 0.779(6) | $^1/_3$ | $^2/_3$ | 0.8063(9) | 0.0007(6) |
| Ir11/Cu11 | 2d | 1.0 | $^1/_3$ | $^2/_3$ | 0.8903(8) | 0.0007(6) |
| Ir12/Cu12 | 2d | 0.779(6) | $^1/_3$ | $^2/_3$ | 0.9820(9) | 0.0007(6) |
| Ir13/Cu13 | 2c | 0.442(4) | 0 | 0 | 0.1231(13) | 0.035(8) |
| Ir14/Cu14 | 3f | 0.147(4) | 0.120(7) | 0 | $^1/_2$ | 0.035(8) |
| Ir15/Cu15 | 6g | 0.147(4) | 0.399(6) | $^2/_3$ | 0.075(2) | 0.035(8) |
| Ir16/Cu16 | 6g | 0.147(4) | 0.392(7) | $^2/_3$ | 0.348(2) | 0.035(8) |
| Ir17/Cu17 | 6g | 0.147(4) | 0.308(8) | $^2/_3$ | 0.7044(16) | 0.035(8) |
| O1 | 3e | | 0.833 | 0 | 0 | 0 |
| O2 | 6g | | 0.698 | 0.174 | 0.991 | 0 |
| O3 | 6g | | 0.048 | 0.176 | 0.079 | 0 |
| O4 | 6g | | 0.851 | 0.339 | 0.069 | 0 |
| O5 | 6g | | 0.334 | 0.512 | 0.125 | 0 |
| O6 | 6g | | 0.654 | 0.155 | 0.144 | 0 |
| O7 | 6g | | 0.036 | 0.164 | 0.185 | 0 |
| O8 | 6g | | 0.353 | 0.830 | 0.208 | 0 |
| O9 | 6g | | 0.795 | 0.343 | 0.243 | 0 |
| O10 | 6g | | 0.859 | 0.077 | 0.267 | 0 |
| O11 | 6g | | 0.335 | 0.499 | 0.292 | 0 |
| O12 | 6g | | 0.033 | 0.173 | 0.360 | 0 |
| O13 | 6g | | 0.825 | 0.317 | 0.340 | 0 |
| O14 | 6g | | 0.833 | 0.985 | 0.445 | 0 |
| O15 | 6g | | 0.515 | 0.747 | 0.405 | 0 |
| O16 | 6g | | 0.627 | 0.152 | 0.421 | 0 |
| O17 | 6g | | 0.347 | 0.829 | 0.487 | 0 |

[a] Ir fraction + Cu fraction = 1, except Ir/Cu14−17, where $\sum$ = 0.333. Space group *P*321; $a$ = 10.145 85(8) Å; $c$ = 29.9574(3) Å; $V$ = 2670.64(6) Å$^3$; Rwpr = 12.44%, Rp = 9.97%; $\chi^2$ = 1.523. No standard deviations for oxygen atomic coordinates are given as they were refined individually and then fixed. $U_{iso}$ for O were fixed at zero.

have trigonal symmetry and are therefore ruled out by our electron diffraction data. These data also showed the absence of a glide plane. Therefore model **a**, which has a glide plane and corresponds to the $n = 2$ phase of the DS series[11] with space group $R\bar{3}c$, may be ruled out. A refinement of model **c**, which lacks a glide plane and may be assigned the space group *R*32, proceeded in a fashion similar to those of the previously described phases. The observed, calculated, and difference diffraction profiles are shown in Figure 13 ($R_{wpr}$ = 11.18%, $\chi^2$ = 1.754), and the refined structural parameters are presented in Table 8. The idealized structure is drawn in Figure 14. It should be noted that this is the same structure that was recently proposed for the "18R" phase $Sr_9Ni_7O_{21}$ observed by TEM.[12]

The inverse molar magnetic susceptibilities of our products, measured at 1000 G, are plotted in Figure 15. The susceptibilities showed no dependence on the

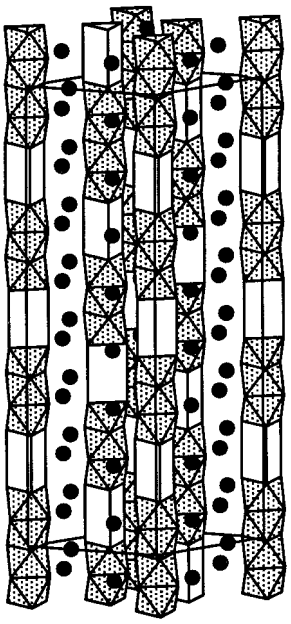

**Figure 12.** Plausible (model **c**) crystal structure of $Ba_{16}Cu_3Ir_{10}O_{39}$. Octahedra are shaded; trigonal prismatic sites are unshaded. Shaded circles represent Ba.

measuring field. The ZFC and FC data were fitted to a Curie−Weiss law with allowance for an additional temperature-independent (TIP) contribution to the susceptibility.

$$\chi_M = \frac{C}{T - \theta} + \alpha$$

In the temperature range 150−300 K the Curie−Weiss law is obeyed well, and the derived values of *C*, $\theta$, and α are shown in Table 9. Values for the related and previously reported phase $Sr_4CuIr_2O_9$ are also given for comparison. In all cases the value of the Curie constant is lower than expected, suggesting the presence of extensive spin-pairing in the cation chains. The negative values of $\theta$ indicate the presence of antiferromagnetic interactions. Due to the cation disorder within polyhedral chains it is difficult to suggest where the spin pairing is occurring.

The electrical resistivities measured at 280 K for our products are shown in Table 10. The $Sr_4CuIr_2O_9$ phase is again included for comparison. All of these phases are insulators, and the general trend is an increase in electrical conductivity with increasing $c_1/c_2$ i.e., with an increasing proportion of iridium. On cooling, the resistivities became immeasurably large.

## Discussion

The powder XRD refinements of all of the structures described above are good enough to demonstrate that it is possible to prepare commensurate target structures in our classification scheme. The large number of variables involved in the refinements of these structures inevitably leads to difficulties, especially in determination of the positions of lighter atoms. Oxygen positions in particular should be regarded only as approximate. The powder XRD data do, however, yield enough information to allow us to identify similarities between these structures and those of $Ba_6CuIr_4O_{15}$ and $Sr_4$-

(11) Campá, J.; Gutiérrez-Puebla, E.; Monge, A.; Rasines, I.; Ruíz-Valero, C. *J. Solid State Chem.* **1996**, *126*, 27.

(12) Huvé, M.; Renard, C.; Abraham, F.; Van Tendeloo, G.; Amelinckx, S. *J. Solid State Chem.* **1998**, *135*, 1.

**Table 7. Atomic Parameters for $Ba_{16}Cu_3Ir_{10}O_{39}$ (Model c)**

| atom | site | Ir fraction[a] | *x* | *y* | *z* | $U_{iso}$/Å$^2$ |
|---|---|---|---|---|---|---|
| Ba1 | 3e | | 0 | 0.328(6) | 0 | 0.0122(5) |
| Ba2 | 6g | | 0.319(4) | 0.335(5) | 0.0645(8) | 0.0122(5) |
| Ba3 | 6g | | 0.003(4) | 0.347(5) | 0.1235(8) | 0.0122(5) |
| Ba4 | 6g | | 0.342(4) | 0.336(4) | 0.1841(7) | 0.0122(5) |
| Ba5 | 6g | | 0.991(4) | 0.327(5) | 0.2518(9) | 0.0122(5) |
| Ba6 | 6g | | 0.335(4) | 0.324(4) | 0.3144(6) | 0.0122(5) |
| Ba7 | 6g | | 0.013(4) | 0.329(4) | 0.3737(8) | 0.0122(5) |
| Ba8 | 6g | | 0.322(5) | 0.334(5) | 0.4399(7) | 0.0122(5) |
| Ba9 | 3f | | 0 | 0.353(5) | 1/2 | 0.0122(5) |
| Ir1/Cu1 | 2c | 1.0 | 0 | 0 | 0.0374(10) | 0.0068(6) |
| Ir2/Cu2 | 2c | 0.714(6) | 0 | 0 | 0.1074(13) | 0.0068(6) |
| Ir3/Cu3 | 2c | 0.714(6) | 0 | 0 | 0.2707(13) | 0.0068(6) |
| Ir4/Cu4 | 2c | 1.0 | 0 | 0 | 0.3471(12) | 0.0068(6) |
| Ir5/Cu5 | 2c | 0.714(6) | 0 | 0 | 0.4197(13) | 0.0068(6) |
| Ir6/Cu6 | 2d | 0.714(6) | 1/3 | 2/3 | 0.0148(13) | 0.0068(6) |
| Ir7/Cu7 | 2d | 1.0 | 1/3 | 2/3 | 0.0893(12) | 0.0068(6) |
| Ir8/Cu8 | 2d | 1.0 | 1/3 | 2/3 | 0.1635(11) | 0.0068(6) |
| Ir9/Cu9 | 2d | 0.714(6) | 1/3 | 2/3 | 0.2355(11) | 0.0068(6) |
| Ir10/Cu10 | 2d | 0.714(6) | 1/3 | 2/3 | 0.3988(14) | 0.0068(6) |
| Ir11/Cu11 | 2d | 1.0 | 1/3 | 2/3 | 0.4726(11) | 0.0068(6) |
| Ir12/Cu12 | 2d | 0.714(6) | 1/3 | 2/3 | 0.5457(12) | 0.0068(6) |
| Ir13/Cu13 | 2d | 0.714(6) | 1/3 | 2/3 | 0.7081(13) | 0.0068(6) |
| Ir14/Cu14 | 2d | 1.0 | 1/3 | 2/3 | 0.7841(11) | 0.0068(6) |
| Ir15/Cu15 | 2d | 0.714(6) | 1/3 | 2/3 | 0.8559(13) | 0.0068(6) |
| Ir16/Cu16 | 2c | 0.571(4) | 0 | 0 | 0.1951(16) | 0.029(7) |
| Ir17/Cu17 | 3f | 0.190(4) | 0.970(14) | 0 | 1/2 | 0.029(7) |
| Ir18/Cu18 | 2d | 0.571(4) | 1/3 | 2/3 | 0.3268(17) | 0.029(7) |
| Ir19/Cu19 | 6g | 0.190(4) | 0.301(8) | 2/3 | 0.6318(18) | 0.029(7) |
| Ir20/Cu20 | 6g | 0.190(4) | 0.410(4) | 2/3 | 0.939(2) | 0.029(7) |
| O1 | 3e | | 0.849 | 0 | 0 | 0 |
| O2 | 6g | | 0.696 | 0.190 | 0.014 | 0 |
| O3 | 6g | | 0.002 | 0.173 | 0.065 | 0 |
| O4 | 6g | | 0.350 | 0.839 | 0.058 | 0 |
| O5 | 6g | | 0.839 | 0.005 | 0.142 | 0 |
| O6 | 6g | | 0.682 | 0.178 | 0.108 | 0 |
| O7 | 6g | | 0.352 | 0.525 | 0.125 | 0 |
| O8 | 6g | | 0.332 | 0.827 | 0.192 | 0 |
| O9 | 6g | | 0.822 | 0.328 | 0.185 | 0 |
| O10 | 6g | | 0.842 | 0.016 | 0.234 | 0 |
| O11 | 6g | | 0.677 | 0.177 | 0.253 | 0 |
| O12 | 6g | | 0.342 | 0.514 | 0.271 | 0 |
| O13 | 6g | | 0.019 | 0.177 | 0.308 | 0 |
| O14 | 6g | | 0.832 | 0.338 | 0.334 | 0 |
| O15 | 6g | | 0.855 | 0.024 | 0.378 | 0 |
| O16 | 6g | | 0.360 | 0.522 | 0.362 | 0 |
| O17 | 6g | | 0.022 | 0.167 | 0.455 | 0 |
| O18 | 6g | | 0.795 | 0.298 | 0.419 | 0 |
| O19 | 6g | | 0.338 | 0.833 | 0.437 | 0 |
| O20 | 6g | | 0.341 | 0.508 | 0.507 | 0 |

[a] Ir fraction + Cu fraction = 1, except Ir/Cu17,19,20, where $\sum = 0.333$. Space group *P*321; $a = 10.136\,43(7)$ Å; $c = 35.0616(3)$ Å; $V = 3119.87(5)$ Å$^3$; Rwpr = 10.43%; Rp = 8.04%; $\chi^2 = 1.041$. No standard deviations for oxygen atomic coordinates are given as they were refined individually and then fixed. $U_{iso}$ for O were fixed at zero.

$CuIr_2O_9$. In a fashion similar to that for $Sr_4CuIr_2O_9$, disorder is introduced by the displacement of $Cu^{2+}$ cations from the 3-fold axis running through the trigonal prism centers, toward the rectangular faces of the prisms. In common with $Ba_6CuIr_4O_{15}$, but in contrast with $Sr_4CuIr_2O_9$, there is substantial disorder in the copper/iridium distribution. Due to the difficulty in accurate placement of oxygen atoms using powder XRD data, it is impossible to say how regular the polyhedra are. It is possible that some are intermediate in character between ideal octahedra and trigonal prisms and are thus able to accommodate either $Cu^{2+}$or $Ir^{4+}$. Another problem is the difficulty in distinguishing between candidate structures for a given composition and unit cell, although our data allow us to discount some structures with reasonable certainty. Simulated data sets suggest that neutron diffraction will yield more detailed structural information, including more accurate oxygen coordinates and a unique description of the chain sequences. A further complication is the possibility of modulation in the structures, despite the fact that they are commensurate. This is suggested by the characteristic intensity distribution of reflections in the electron diffraction patterns and the contrast modulation in the lattice images. The origin of the modulation in these structures remains an open question. A recent report of incommensuration in the related phase $Sr_4Ni_3O_9$ [12] was accounted for in terms of the occasional but systematic insertion or removal of single octahedra in the polyhedral chains. However, our electron diffraction patterns indicate commensurate materials, so the above description cannot be the cause of the modulation in our phases. It is possible that it is similar in nature to that studied in $Ba_x(Cu,Pt)O_3$ [13] and $Sr_{1.145}TiS_3$,[14] where there is a pseudoperiodic rotation of triangles of

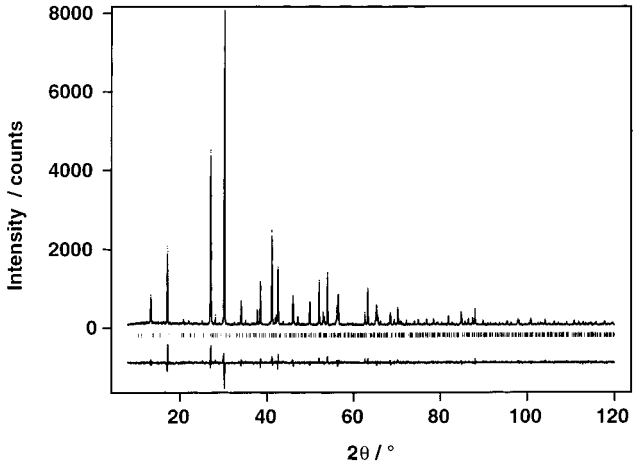


**Figure 13.** Observed, calculated, and difference X-ray diffraction profiles of $Ba_9Cu_2Ir_5O_{21}$. Reflection positions are marked.

**Table 8. Atomic Parameters for $Ba_9Cu_2Ir_5O_{21}$ (Model c)**

| atom | site | Ir fraction[a] | *x* | *y* | *z* | $U_{iso}$/Å$^2$ |
|---|---|---|---|---|---|---|
| Ba1 | 9d | | 0 | 0.3572(14) | 0 | 0.0145(5) |
| Ba2 | 18f | | 0.3265(12) | 0.3369(12) | 0.0561(3) | 0.0145(5) |
| Ba3 | 18f | | 0.0140(12) | 0.3316(12) | 0.1115(3) | 0.0145(5) |
| Ba4 | 9e | | 0.3510(14) | 0.3510(14) | 0.5 | 0.0145(5) |
| Ir1/Cu1 | 6c | 0.905(4) | 0 | 0 | 0.0746(3) | 0.0085(7) |
| Ir2/Cu2 | 6c | 0.905(4) | 0 | 0 | 0.1401(4) | 0.0085(7) |
| Ir3/Cu3 | 6c | 0.905(4) | 0 | 0 | 0.2108(4) | 0.0085(7) |
| Ir4/Cu4 | 6c | 0.905(4) | 0 | 0 | 0.3559(3) | 0.0085(7) |
| Ir5/Cu5 | 6c | 0.905(4) | 0 | 0 | 0.4281(4) | 0.0085(7) |
| Ir6/Cu6 | 9d | 0.079(4) | 0.933(4) | 0 | 0 | 0.039(7) |
| Ir7/Cu7 | 6c | 0.237(11) | 0 | 0 | 0.2897(8) | 0.039(7) |
| Ir8/Cu8 | 9e | 0.079(4) | 0.103(4) | 0 | 0.5 | 0.039(7) |
| O1 | 18f | | 0.982 | 0.150 | 0.045 | 0.009(3) |
| O2 | 18f | | 0.856 | 0.033 | 0.111 | 0.009(3) |
| O3 | 18f | | 0.990 | 0.173 | 0.171 | 0.009(3) |
| O4 | 18f | | 0.828 | 0.970 | 0.251 | 0.009(3) |
| O5 | 18f | | 0.851 | 0.994 | 0.322 | 0.009(3) |
| O6 | 18f | | 0.029 | 0.160 | 0.393 | 0.009(3) |
| O7 | 18f | | 0.835 | 0.992 | 0.454 | 0.009(3) |

[a] Ir fraction + Cu fraction = 1, except Ir/Cu6,8, where $\sum = 0.333$. Space group *R*32; $a = 10.144\,64(11)$ Å; $c = 38.2455(6)$ Å, $V = 3408.66(10)$ Å$^3$; Rwpr = 11.18%; Rp = 8.87%; $\chi^2 = 1.754$. No standard deviations for oxygen atomic coordinates are shown as they were refined individually and then fixed.

(13) Ukei, K.; Yamamoto, A.; Watanabe, Y.; Shishido, T.; Fukuda, T. *Acta Crystallogr. B* **1993**, *49*, 67.
(14) Onoda, M.; Saeki, M.; Yamamoto, A.; Kato, K. *Acta Crystallogr. B* **1993**, *49*, 929.

**Table 9. Magnetic Parameters of Ba/Cu/Ir/O Phases**

| compd | $c_1/c_2$ | $C$/(emu K mol$^{-1}$) | $\mu_{eff}(obs)/\mu_B$ | $\mu_{eff}(calc)^a/\mu_B$ | $\theta$/K | $\alpha$/(emu mol$^{-1}$) |
|---|---|---|---|---|---|---|
| $Ba_{16}Cu_3Ir_{10}O_{39}$ | 1.6250 | 1.83 | 3.83 | 6.24 | −144 | 0.003 76 |
| $Ba_5CuIr_3O_{12}$ | 1.6000 | 0.573 | 2.14 | 3.46 | −98 | 0.001 79 |
| $Ba_{14}Cu_3Ir_8O_{33}$ | 1.5714 | 2.18 | 4.18 | 5.74 | −136 | 0.004 10 |
| $Ba_9Cu_2Ir_5O_{21}$ | 1.5556 | 1.19 | 3.09 | 4.58 | −72 | 0.001 84 |
| $Sr_4CuIr_2O_9$ | 1.5000 | 0.396 | 1.78 | 3.00 | −7.5 | 0.000 69 |

[a] Calculated value of $\mu_{eff}$, assuming no spin-pairing.

**Table 10. Electrical Resistivity Data for Ba/Cu/Ir/O Phases**

| compd | $c_1/c_2$ | $c_1$ | $c_2$ | $\rho$/(Ω cm) |
|---|---|---|---|---|
| $Ba_{16}Cu_3Ir_{10}O_{39}$ | 1.6250 | 4.383 | 2.696 | 500 |
| $Ba_5CuIr_3O_{12}$ | 1.6000 | 4.329 | 2.706 | 329 |
| $Ba_{14}Cu_3Ir_8O_{33}$ | 1.5714 | 4.280 | 2.723 | 3220 |
| $Ba_9Cu_2Ir_5O_{21}$ | 1.5556 | 4.245 | 2.728 | 9060 |
| $Sr_4CuIr_2O_9$ | 1.5000 | 4.033 | 2.689 | 132000 |

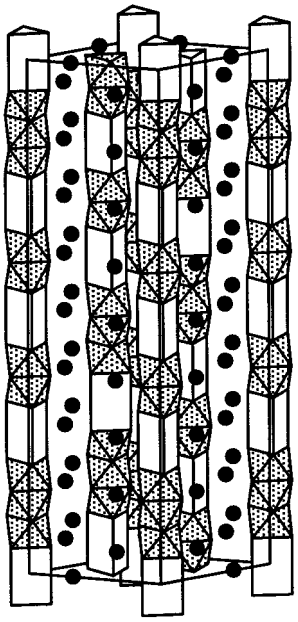

**Figure 14.** Idealized crystal structure of $Ba_9Cu_2Ir_5O_{21}$. Octahedra are shaded; trigonal prismatic sites are unshaded. Shaded circles represent Ba.

anions along $c_2$, inducing a modulation of the Ba/Sr cation positions in a helical fashion along $c_1$. In our materials the period of the modulation has to be commensurate with the overall $c$ parameter. Our structural refinements using XRD data do not allow for the presence of a modulation, the nature of which may be elucidated in the future by a detailed consideration of neutron diffraction intensities using the superspace group approach.

In our structure prediction scheme it might seem contradictory to use the composite crystal unit cell parameters $c_1$ and $c_2$ in order to find the number of layers in a commensurate unit cell. However, the fact that it is possible to prepare several of the phases predicted in this manner shows that the approach is beneficial. We believe that all structures in this family are probably best envisaged as composite crystals. The commensurate structures are then a special case for which the layered description is useful. We have systematically listed all possible commensurate structures in the structural family with up to 18 layers ($p \leq 9$ in Table 2). All the structures reported to date are accounted for, along with the members $n = 5$, 6, 9, and 15 of the DS series and several new structures. Other members of the DS series with $n > 3$ have more than 18 layers per unit cell and are not described here. Some compositions have more than one possible sequence of octahedra and trigonal prisms in a chain and several possible chain translations, and, as yet, it is difficult to formulate any rule as to which structure is most likely to form. It should be noted that compounds with compositions corresponding to members $n = 1$, 2, and 5 of the DS series have 2, 5, and 3 possible structures, respectively, only one of which fits into the DS series in each case. However, the DS structures for these three compositions have the highest symmetry (rhombohedral rather than trigonal), and from our observations it seems likely that rhombohedral structures are formed preferentially. Electron diffraction patterns with rhombohedral rather than trigonal symmetry are obtained for $Ba_9Cu_2Ir_5O_{21}$ and the previously reported $Ba_6CuIr_4O_{15}$ ($n = 1$). There is no limit to the number of commensurate structures which can be envisaged with more than 18 layers per unit cell, but the likelihood of stacking faults increases with the number of layers and structural refinement becomes more difficult due to the large number of variables in trigonal cells (only structures with multiples of six layers can have rhombohedral symmetry). If all commensurate phases are found to be modulated, as is possible, then the layered model becomes redundant and the composite crystal model with four-dimensional symmetry should always be applied in structural studies. The concept of modulation in this structure type is a relatively new idea, and the only example of an oxide for which this has been fully investigated is $Ba_x(Cu,Pt)O_3$.[13] It would be futile to concentrate on commensurate structures if the family is actually one of metastable and modulated composite crystals with a continuous range of $c_1/c_2$ ratios. Structures of this type are perhaps better classified by their $c_1/c_2$ ratios, and their commensurability is probably irrelevant to their electronic properties. However, these comments are based only on our investigations of phases containing iridium, and it remains to be seen how the structural and electronic properties are affected by the substitution of different cations.

In our investigation we could not produce iridium-containing compounds covering the whole range of the series ($4/3 \leq c_1/c_2 \leq 2$). The upper limit to the obtainable $c_1/c_2$ ratio is around 1.70, and ratios below about 1.55 were not observed in our experiments (although when strontium is used instead of barium the phases $Sr_4CuIr_2O_9$ with $c_1/c_2 = 1.5$ and $Sr_3CuIrO_6$ with $c_1/c_2 = 4/3$ may be prepared). The fact that phases with ratios greater than 1.7 cannot be prepared is unsurprising given that $BaIrO_3$ adopts[15] a 9R structure rather than a 2H structure. It is likely that cations such as $Mn^{4+}$

(15) Powell, A. V.; Battle, P. D. *J. Alloys Compd.* **1993**, *191*, 313.

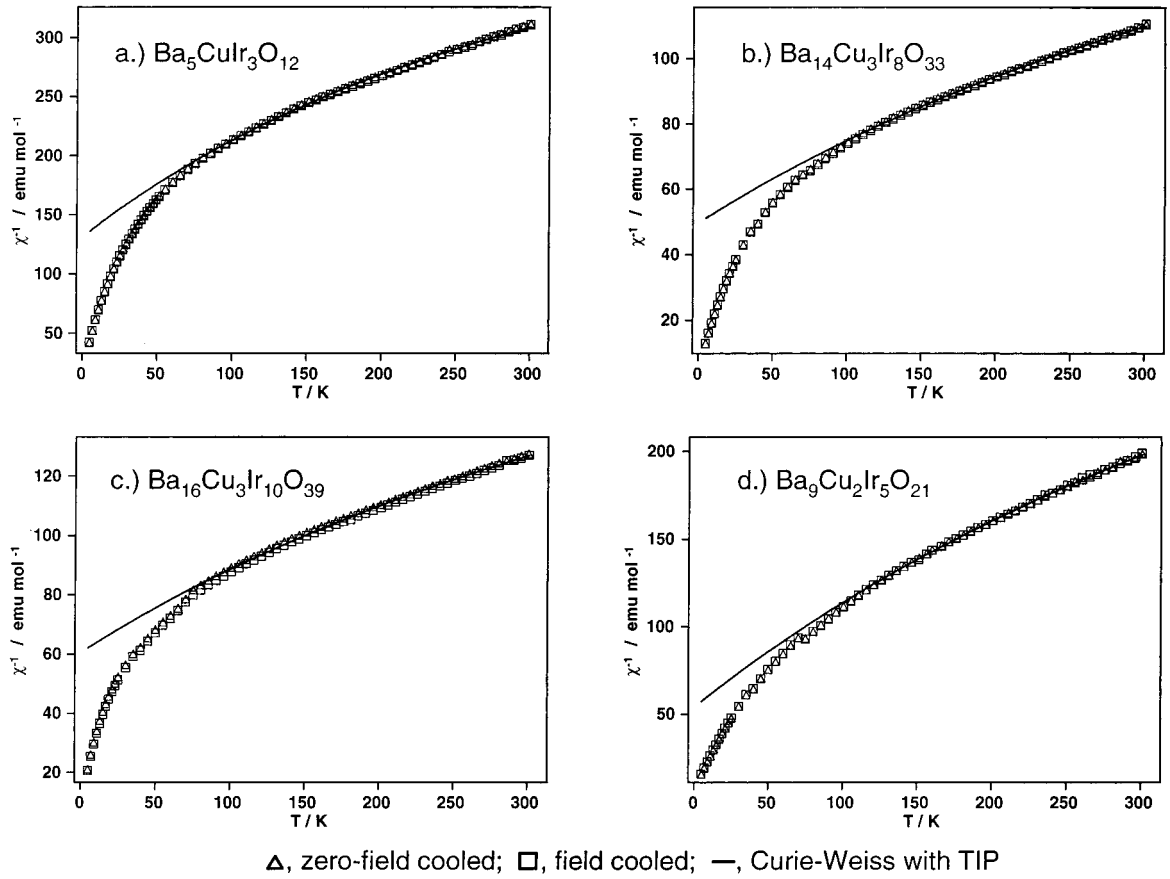


**Figure 15.** Temperature dependence of the inverse ZFC and FC molar magnetic susceptibilities, measured in a field of 1000 G, of (a) $Ba_5CuIr_3O_{12}$, (b) $Ba_{14}Cu_3Ir_8O_{33}$, (c) $Ba_{16}Cu_3Ir_{10}O_{39}$, and (d) $Ba_9Cu_2Ir_5O_{21}$. Fits to a modified Curie−Weiss law are shown.

and $Ni^{4+}$ which occur in the 2H structure ($c_1/c_2 = 2.0$) could be incorporated into structures with a ratio greater than 1.7. Our investigations have always shown the $c_1/c_2$ ratio to decrease continuously with heating, illustrating the flexibility of the system. To obtain a phase with the desired ratio, the reaction mixture must be fired for exactly the correct length of time (higher temperatures have the effect of decreasing $c_1/c_2$ more quickly); naturally some trial and error is required in order to find the optimum preparation conditions, to ensure purity and good crystallinity before $c_1/c_2$ reaches the desired value. There appears to be no particular ratio at which phases are thermodynamically stable, apart from the $Sr_3CuIrO_6$ end-member ($c_1/c_2 = 4/3$), which always formed as an impurity in our previously reported investigation of $Sr_4CuIr_2O_9$,[2] when samples were heated for too long.

The magnetic susceptibilities of all our phases are lower than expected, but because of the apparent cation disorder in the structures it is impossible to comment on where spin-pairing is occurring. The lack of long-range magnetic ordering could be a consequence of the cation disorder. All of our phases are insulators, but the electrical conductivity increases with $c_1/c_2$, i.e., as the proportion of iridium in the structure increases. This is not unexpected given the diffuse nature of the iridium 5d orbitals relative to the copper 3d orbitals. An example of a compound containing a higher proportion of iridium than our phases is $BaIrO_{3-\delta}$, $Ir^{4+}$ being found in trimers of face-sharing octahedra.[15] This compound displays high electrical conductivity which is metallic in nature. It will be interesting to investigate the electronic properties of phases containing cations other than iridium and copper and to see whether there is enhanced electrical conductivity or dependence of magnetic properties on the $c_1/c_2$ ratio.

**Acknowledgment.** We are grateful to EPSRC for financial support and to Jacques Darriet for many stimulating discussions.

CM980317M